 DOI:10.30420/566414044

A Model Predictive Method for Specific Harmonic Reduction at Low Switching Frequency in Permanent Magnet Synchronous Motor

Tianyu Yuan[1], Xiaoguang Zhang[1], Yuanhang Cao[1]
[1] North China University of Technology, China

Corresponding author: Xiaoguang Zhang, zxg@ncut.edu.cn
Speaker: Tianyu Yuan, 2023312080106@mail.ncut.edu.cn

Abstract

For the model predictive control process of permanent magnet synchronous motors (PMSM) in the limit of low switching frequency, the low harmonics in the motor stator current have a detrimental effect on the PMSM drive system. Therefore, it is necessary to reduce the percentage of specific low harmonics under the above control method. In this paper, a model predictive specific harmonic reduction control (MPSHRC) method based on the dq axes currents is proposed, which is significant for 5^{th} and 7^{th} harmonic reduction at low switching frequencies.

1 Introduction

Permanent magnet synchronous motors (PMSMs) have recently found initial applications in industry and production. Their power density is higher than that of asynchronous motors and they have a larger starting pitch thus supporting permanent magnet direct drive technology, which can reduce production costs and improve economic efficiency in industrial production [1-2].

However, the mainstream PMSM control methods are still those originally applied to induction motors, i.e., Field-Oriented Control (FOC), Direct Torque Control (DTC), etc., and most of them use Proportional Integral Derivative (PID) control techniques for their feedback links. It should be noted that the above control methods are not fully applicable to the steady state process of PMSM, which makes the advantages of PMSM poorly reflected [3].

Model Predictive Control (MPC) techniques are more advanced than traditional PID control techniques and have gained importance through the advantages of not requiring PID devices and avoiding the cascade structure in linear control schemes [4-5].

MPC appeared in the 1960s, initially due to the limitation of time constants, MPC was applied to lower switching frequency and high-power occasions in the industrial field. Due to the rapid development of digital processing technology in recent years, many scholars have further deepened the MPC concept based on the algorithmic framework of high control frequency, such as improving the control accuracy [6-7], using continuous control set, and so on. However, the above algorithms are difficult to be applied to high-power occasions because while improving the control effect, they further increase the switching frequency, which increases the switching loss of the switching devices [8-10], which, from the practical point of view, raises the risk of damage to the devices [11-12]. At the same time, as the switching frequency is limited on line, more harmonic contents will appear in the current driving the PMSM, and these harmonic contents are dominated by low harmonics (e.g., 5th,7th). The presence of low harmonics causes large torque pulsations in the PMSM and also interferes with the normal amount of feedback from the motor, which is a bad effect on the control system side, and the motor side [13-15].

In this paper, a harmonic suppression algorithm based on model predictive control is proposed based on the above problem. Firstly, specific low order harmonics are extracted from the current after one beat delay using a harmonic extractor, then the harmonic current components at the next moment are predicted in the PMSM equations considering harmonics, which are then embedded into a cost function along with a finite-set traversal of the fundamental current and frequency limiting terms of the conventional model, and finally an appropriate switching signal is output. Ultimately, the proposed MPSHRC algorithm in this paper attenuates the lower harmonic components and reduces the overall THD of the system, thus improving the control effectiveness of PMSM.

The structure of this paper is divided as follows: the ideal PMSM model is given in section 2, the conventional Low Switching Frequency Model Predictive Current Control Algorithm (LSF-MPCC) is presented in section 3, the proposed (MPSHRC) algorithm is introduced in section 4, the proposed MPSHRC algorithm is validated by simulation in section 5, and finally, the overall conclusion is given in section 6.

ISBN 978-3-8007-6414-3

2 Mathematical Model of PMSM

In this paper, the study is carried out using surface PMSM (SPMSM). The system framework is shown in Fig. 1, where the DC bus generates three-phase AC power through a two-point flat three-phase inverter to supply the SPMSM.

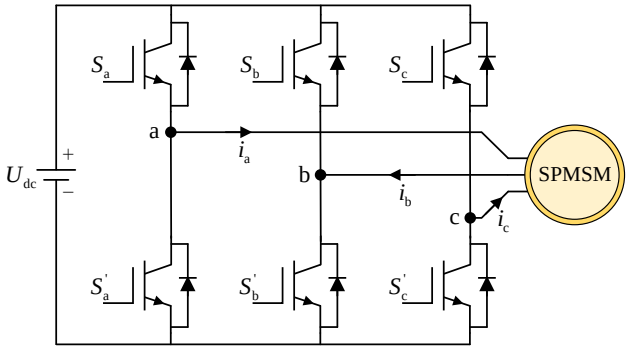

Fig. 1. Main circuit of PMSM drive system

where S_a, S_b, S_c are the upper bridge arms of the three-phase inverter and S'_a, S'_b, S'_c are the lower bridge arms of the three-phase inverter, and the switching states of the lower bridge arms are always opposite to the switching states of the upper bridge arms.

By traversing the different switching states of S_a, S_b, S_c, a set of 8 voltage vectors can be obtained, which is represented in the complex plane as Fig. 2.

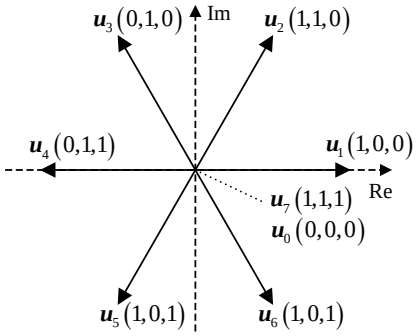

Fig. 2. 8 finite set voltage vectors in complex plane

For the convenience of the study, the three-phase voltages of the PMSM are decoupled according to the similar DC motor excitation and rotor voltages, and the voltage equation of the SPMSM in the dq axes is obtained as

$$\begin{cases} u_d = Ri_d + L\dfrac{di_d}{dt} - \omega_e L i_q \\ u_q = Ri_q + L\dfrac{di_q}{dt} + \omega_e L i_d + \omega_e \psi_f \end{cases} \tag{1}$$

where i_d and i_q represent the dq axes current, R represents the stator resistance, L represents the stator inductance, ω_e represents the electrical angular velocity, and ψ_f is the rotor magnetic flux.

3 Traditional LSF-MPCC Method

The program block diagram of the traditional LSF-MPCC method (T-LSF-MPCC) is shown in Fig. 3.

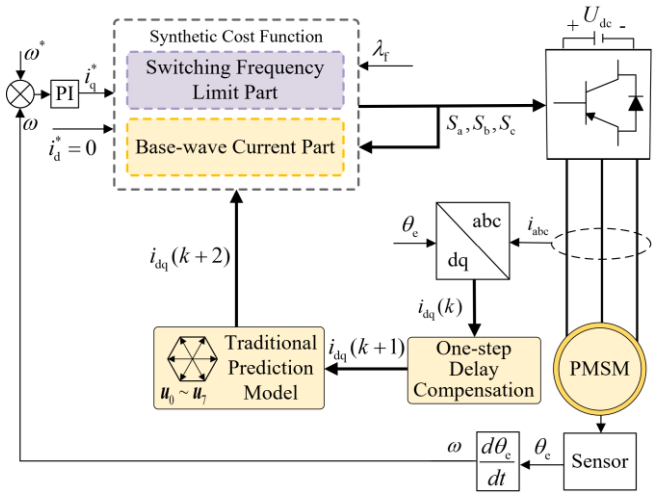

Fig. 3. Block diagram of T-LSF-MPCC Method

Evaluating (1) for the next moment using the Euler forward method, the dq axes current for the next moment can be written as

$$\begin{cases} i_d^p(k+1) = (1-\dfrac{T_s R}{L})i_d(k) + \dfrac{T_s}{L}u_d(k) + T_s\omega_e i_q(k) \\ i_q^p(k+1) = (1-\dfrac{T_s R}{L})i_q(k) + \dfrac{T_s}{L}u_q(k) - T_s\omega_e i_d(k) - \dfrac{T_s\omega_e\psi_f}{L} \end{cases} \tag{2}$$

where T_s represents the control period of the system.

Due to the non-negligible delay during the actual program operation, it is necessary to carry out a one-beat delay of the current moment current $\boldsymbol{i}_{dq}(k)$ in accordance with (2) to obtain $\boldsymbol{i}_{dq}^p(k+1)$. Then, the predicted current $\boldsymbol{i}_{dq}^p(k+2)$ is calculated by substituting $\boldsymbol{i}_{dq}^p(k+1)$ into (2) again, denoted as

$$\begin{cases} i_d^p(k+2) = (1-\dfrac{T_s R}{L})i_d(k+1) \\ \qquad + \dfrac{T_s}{L}u_d(k) + T_s\omega_e i_q(k+1) \\ i_q^p(k+2) = (1-\dfrac{T_s R}{L})i_q(k+1) \\ \qquad + \dfrac{T_s}{L}u_q(k) - T_s\omega_e i_d(k+1) - \dfrac{T_s\omega_e\psi_f}{L} \end{cases} \tag{3}$$

Then, the switching value $S_a(k-1), S_b(k-1), S_c(k-1)$ of the three-phase upper bridge arm of the inverter of the previous moment is extracted. The $\boldsymbol{i}_{dq}^p(k+2)$,the given quantity $\boldsymbol{i}_{dq}^*$, the switching frequency limiting weight λ_f , and $S_a(k-1), S_b(k-1), S_c(k-1)$ are brought into the cost function, and the voltage vector that makes the smallest resultant value is taken for the output of the next moment by traversing the finite set consisting of 8

voltage vectors. The above cost function can be expressed as

$$\begin{cases} J^{\mathrm{T}} = g_{\mathrm{b}}^{\mathrm{T}} + g_{\mathrm{s}}^{\mathrm{T}} \\ g_{\mathrm{b}}^{\mathrm{T}} = \left[i_{\mathrm{d}}^{*} - i_{\mathrm{d}}^{\mathrm{p}}(k+2) \right]^2 + \left[i_{\mathrm{q}}^{*} - i_{\mathrm{q}}^{\mathrm{p}}(k+2) \right]^2 \\ g_{\mathrm{s}}^{\mathrm{T}} = \lambda_{\mathrm{f}} \sum_{i=a,b,c} \left| S_i(k) - S_i(k-1) \right| \end{cases} \tag{4}$$

where $S_i(k)$ represents the switching state of the traversing vector. $g_{\mathrm{b}}^{\mathrm{T}}$ corresponds to Switching Frequency Limit Part in Fig. 3, and $g_{\mathrm{s}}^{\mathrm{T}}$ corresponds to Base-wave Current Part in Fig. 3.

4 Proposed MPSHRC Method

This section provides a detailed description of the proposed MPSHRC method. Firstly, the harmonic currents of a given number of times in the stator current are extracted, then substituted into a prediction model considering harmonic currents for the prediction of harmonic currents at the moment *k+2*, and finally, a Synthetic Cost Function is constructed to determine the issued voltage vector, thus reducing the adverse effects of low harmonic currents on the system. The overall control block diagram of the system can be given by Fig.4.

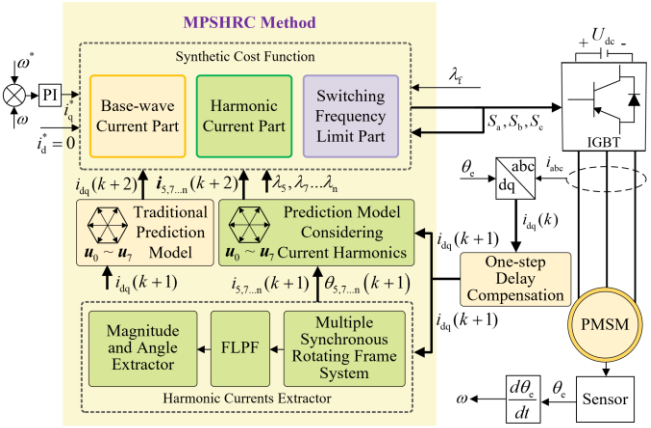

Fig. 4. Block diagram of proposed MPSHRC Method

4.1 Harmonic Current Extractor

The PMSM stator current i_{abc} is compensated by the one-tap delay described in (3) to obtain $i_{\mathrm{dq}}(k+2)$, which contains the fundamental current $i_{\mathrm{d}}^{'}, i_{\mathrm{q}}^{'}$ and the various harmonic currents $i_{\mathrm{d}}^{5}, i_{\mathrm{q}}^{5}, i_{\mathrm{d}}^{7}, i_{\mathrm{q}}^{7} \ldots i_{\mathrm{d}}^{n}, i_{\mathrm{q}}^{n}$. Therefore, a harmonic current extractor needs to be designed to extract the harmonic current components.

Firstly, the PMSM model considering harmonics is given, then $i_{\mathrm{dq}}(k+2)$ is transformed back to the $\alpha\beta$ coordinate system, and the $\alpha\beta$ components corresponding to the rotational speeds of different harmonics are extracted through the Multiple Synchronous Rotating Frame System (MSRFS), then the harmonic current components under the dq axes coordinate system are generated through the first-order low-pass filter(FLPF), and finally the amplitude and angle of the harmonic currents are calculated under the dq axes coordinate system.

4.1.1 PMSM Current Equation Considering Harmonics

It should be noted that the equations listed in (1) are idealized dq axes currents after converting the PMSM stator currents to the dq axes, which is obviously not optimized for harmonic currents. Therefore, a specific number of harmonic current terms need to be added to the ideal model. Fig. 5 gives a schematic diagram of the PMSM stator current containing all the $6k \pm 1^{\mathrm{th}}$ current harmonics in the $\alpha\beta$ coordinate system.

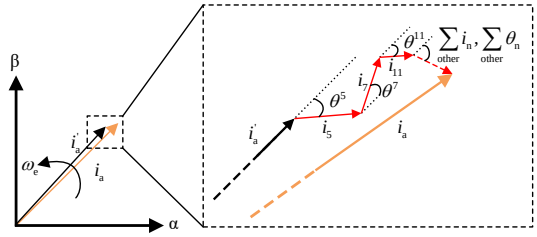

Fig. 5. PMSM stator current with all $6k \pm 1$ current harmonics in the $\alpha\beta$ axes

Therefore, the dq current expression of the PMSM considering harmonics is given by

$$\begin{cases} i_{\mathrm{d}} = i_{\mathrm{d}}^{'} + \sum_{n=6k\pm1, k\geq1}^{k\to\infty} i_{\mathrm{d}}^{n} \\ i_{\mathrm{q}} = i_{\mathrm{q}}^{'} + \sum_{n=6k\pm1, k\geq1}^{k\to\infty} i_{\mathrm{q}}^{n} \end{cases} \tag{5}$$

Based on [16], the above equation can be rewritten in the form of the relationship between magnitude and angle as

$$\begin{cases} i_{\mathrm{d}} = i_1 \cos\theta_1 + \sum_{n=6k\pm1, k\geq1}^{k\to\infty} i_n \cos\left(6k\omega_{\mathrm{e}}t + \theta_n\right) \\ i_{\mathrm{q}} = i_1 \sin\theta_1 + \sum_{n=6k\pm1, k\geq1}^{k\to\infty} i_n \sin\left(6k\omega_{\mathrm{e}}t + \theta_n\right) \end{cases} \tag{6}$$

Referring to the FFT results of Fig.9, Fig.11, this paper only suppresses the more obvious 5th and 7th harmonic currents in the program. And it should be noted that this method is not limited to the 5th and 7th harmonic currents, but can add or remove any number of harmonic currents with great flexibility. Thus (6) can continue to be rewritten as

$$\begin{cases} i_{\mathrm{d}} = i_{\mathrm{d}}^{'} + i_{\mathrm{d}}^{5} + i_{\mathrm{d}}^{7} \\ i_{\mathrm{q}} = i_{\mathrm{q}}^{'} + i_{\mathrm{q}}^{5} + i_{\mathrm{q}}^{7} \end{cases} \tag{7}$$

$$\begin{cases} i_{\mathrm{d}} = i_1 \cos\theta_1 + i_5 \cos\left(6\omega_{\mathrm{e}}t + \theta_5\right) + i_7 \cos\left(6\omega_{\mathrm{e}}t + \theta_7\right) \\ i_{\mathrm{q}} = i_1 \sin\theta_1 + i_5 \sin\left(6\omega_{\mathrm{e}}t + \theta_5\right) + i_7 \sin\left(6\omega_{\mathrm{e}}t + \theta_7\right) \end{cases} \tag{8}$$

According to the above equation, the 5th current harmonic and the 7th current harmonic are expressed as

the $6\omega_e$ th AC component in the dq axes coordinate system rotating at the fundamental angular velocity ω_e. Therefore, the dq axes voltage equation described in (8) is finally updated as

$$\begin{cases} u_d = R\left(i_d^{'} + i_d^5 + i_d^7\right) \\ \quad + L\left(\dfrac{d}{dt}\left(i_d^{'} + i_d^5 + i_d^7\right) - \omega_e\left(i_q^{'} + i_q^5 + i_q^7\right)\right) \\ u_q = R\left(i_q^{'} + i_q^5 + i_q^7\right) + \\ \quad + L\left(\dfrac{d}{dt}\left(i_q^{'} + i_q^5 + i_q^7\right) + \omega_e\left(i_d^{'} + i_d^5 + i_d^7\right)\right) + \omega_e\psi_f \end{cases} \tag{9}$$

4.1.2 Multiple Synchronous Rotating Frame System

The MSRFS [16-18] method is used in this paper for the effective extraction of current harmonics. The MSRFS method is shown in Fig.6.

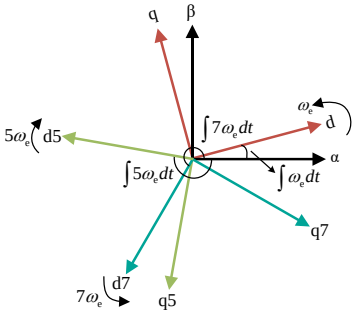

Fig. 6. MSRFS Method

In this case, the fundamental dq axes coordinate system is rotated counterclockwise at an electrical angular velocity ω_e, the $6k+1^{\text{th}}$ dq axes coordinate system is rotated in the same direction as the fundamental coordinate system, and the $6k-1^{\text{th}}$ coordinate system is rotated in the opposite direction of the fundamental coordinate system. The rotational direction of the fundamental dq axes coordinate system is the same as that of the fundamental dq axes coordinate system. Therefore, the transformation equation for transforming the fundamental αβ axes current to the dq axes current in the 5th,7th coordinate system can be obtained as

$$\begin{bmatrix} i_d^{5F} \\ i_q^{5F} \\ i_d^{7F} \\ i_q^{7F} \end{bmatrix} = \begin{bmatrix} \cos(5\omega_e t) & -\sin(5\omega_e t) \\ \sin(5\omega_e t) & \cos(5\omega_e t) \\ \cos(7\omega_e t) & \sin(7\omega_e t) \\ -\sin(7\omega_e t) & \cos(7\omega_e t) \end{bmatrix} \begin{bmatrix} i_\alpha \\ i_\beta \end{bmatrix} \tag{10}$$

4.1.3 Calculation of Harmonic Currents in Each dq axes

Fig.7 gives the FFT analysis of i_q^{5F} of the motor at 2000rad/min,5N.m. Where the DC component represents the amount of current corresponding to the number of harmonics, while the source of the AC component is the other currents except the 5th harmonic current, where the largest fundamental current component behaves as the 6th harmonic in the 5,7 synchronous rotation coordinate system.

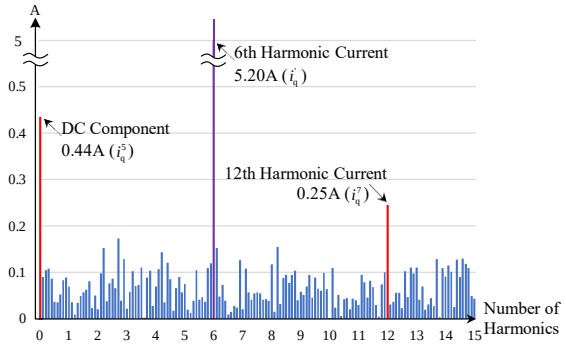

Fig. 7. FFT analysis of i_q^{5F}

In this paper, the FLPF method is used for the extraction. the FLPF is actually a first order system and the input-output relation equation of the FLPF after backward Eulerian discretization is

$$y(k) = \frac{2\pi f_n T_s}{1+2\pi f_n T_s} x(k) + \frac{1}{1+2\pi f_n T_s} y(k-1) \tag{11}$$

where $y(k)$ and $y(k-1)$ represent the output values at the k^{th},k-1^{th} moment, $x(k)$ represents the input value at the k^{th} moment, f_n is the cutoff frequency of the FLPF, and T_s is the control period. In this paper, the cutoff frequency is set to run at 10 Hz, which is much lower than the 6th harmonic frequency in the synchronous rotating coordinate system. Vectors synthesized from 5th,7th dq axes harmonic currents are $\boldsymbol{i}_5$ and $\boldsymbol{i}_7$, which can be calculated by

$$\begin{cases} i_5 = \sqrt{\left(i_d^5\right)^2 + \left(i_q^5\right)^2}, i_7 = \sqrt{\left(i_d^7\right)^2 + \left(i_q^7\right)^2} \\ \theta_5 = \arctan\dfrac{i_q^5}{i_d^5}, \theta_7 = \arctan\dfrac{i_q^7}{i_d^7} \\ \boldsymbol{i}_5 = i_5 e^{j\theta_5}, \ \boldsymbol{i}_7 = i_7 e^{j\theta_7} \end{cases} \tag{12}$$

where i_5, i_7 denote the amplitude of the harmonic current vector and θ_5, θ_7 denote the angle of the harmonic current vector.

4.2 Harmonic Current Prediction

In Section 3, the harmonic current amplitude and phase angle for a specific number of times at moment *k+1* have been calculated. The harmonic current prediction for the next moment is performed using the PMSM current equation considering harmonics, which results in a

prediction similar to the fundamental current. The harmonic current prediction is divided into two parts, i.e., Prediction Model Considering Current Harmonics and Traditional Prediction Model.

4.2.1 Prediction Model Considering Current Harmonics

According to the equations listed in (7), (8), the PMSM current equation considering harmonics contains three kinds of harmonic currents i_1, i_5, i_7 . According to the above harmonic current relations listed in (12), the expressions for the dq axes currents $i_{\mathrm{d}}^{'}$ and $i_{\mathrm{q}}^{'}$ of i_1 can be obtained as

$$\begin{cases} i_{\mathrm{d}}^{'} = i_{\mathrm{d}} - i_5 \cos\left(6\theta_{\mathrm{e}} + \theta_5\right) - i_7 \cos\left(6\theta_{\mathrm{e}} + \theta_7\right) \\ i_{\mathrm{q}}^{'} = i_{\mathrm{q}} + i_5 \sin\left(6\theta_{\mathrm{e}} + \theta_5\right) - i_7 \sin\left(6\theta_{\mathrm{e}} + \theta_7\right) \end{cases} \tag{13}$$

According to the harmonic model (9), using the Euler forward discretization equation, the 5th,7th harmonic dq axes current expression can be obtained as

$$\begin{cases} i_{\mathrm{d}}^{5\mathrm{p}}(k+2) = i_{\mathrm{d}}^{5}(k) - T_{\mathrm{s}}\left(\dfrac{d\left(i_{\mathrm{d}}^{'\mathrm{p}} + i_{\mathrm{d}}^{7\mathrm{p}}\right)}{dt}\right) \\ \qquad + T_{\mathrm{s}}\left(\dfrac{u_{\mathrm{d}} - Ri_{\mathrm{d}}^{\mathrm{p}}(k+1) + \omega_{\mathrm{e}} L i_{\mathrm{q}}^{\mathrm{p}}(k+1)}{L}\right) \\ i_{\mathrm{q}}^{5\mathrm{p}}(k+2) = i_{\mathrm{q}}^{5}(k) - T_{\mathrm{s}}\left(\dfrac{d\left(i_{\mathrm{q}}^{'\mathrm{p}} + i_{\mathrm{q}}^{7\mathrm{p}}\right)}{dt}\right) \\ \qquad + T_{\mathrm{s}}\left(\dfrac{u_{\mathrm{d}} - Ri_{\mathrm{q}}^{\mathrm{p}}(k+1) - \omega_{\mathrm{e}}\left(Li_{\mathrm{d}}^{\mathrm{p}}(k+1) + \psi_{\mathrm{f}}\right)}{L}\right) \\ i_{\mathrm{d}}^{7\mathrm{p}}(k+2) = i_{\mathrm{d}}^{7}(k) - T_{\mathrm{s}}\left(\dfrac{d\left(i_{\mathrm{d}}^{'\mathrm{p}} + i_{\mathrm{d}}^{5\mathrm{p}}\right)}{dt}\right) \\ \qquad + T_{\mathrm{s}}\left(\dfrac{u_{\mathrm{d}} - Ri_{\mathrm{d}}^{\mathrm{p}}(k+1) + \omega_{\mathrm{e}} L i_{\mathrm{q}}^{\mathrm{p}}(k+1)}{L}\right) \\ i_{\mathrm{q}}^{7\mathrm{p}}(k+2) = i_{\mathrm{q}}^{7\mathrm{p}}(k+1) - T_{\mathrm{s}}\left(\dfrac{d\left(i_{\mathrm{q}}^{'\mathrm{p}} + i_{\mathrm{q}}^{5\mathrm{p}}\right)}{dt}\right) \\ \qquad + T_{\mathrm{s}}\left(\dfrac{u_{\mathrm{d}} - Ri_{\mathrm{q}}^{\mathrm{p}}(k+1) - \omega_{\mathrm{e}}\left(Li_{\mathrm{d}}^{\mathrm{p}}(k+1) + \psi_{\mathrm{f}}\right)}{L}\right) \end{cases} \tag{14}$$

where the derivative of each harmonic is defined as the value of the harmonic current derivative at the previous moment, which can be expressed as

$$\begin{cases} \dfrac{di_{\mathrm{d}}^{'\mathrm{p}}}{dt} = \dfrac{i_{\mathrm{d}}^{'\mathrm{p}}(k+1) - i_{\mathrm{d}}^{'}(k)}{T_{\mathrm{s}}}, \dfrac{di_{\mathrm{q}}^{'\mathrm{p}}}{dt} = \dfrac{i_{\mathrm{q}}^{'\mathrm{p}}(k+1) - i_{\mathrm{q}}^{'}(k)}{T_{\mathrm{s}}} \\ \dfrac{di_{\mathrm{d}}^{5\mathrm{p}}}{dt} = \dfrac{i_{\mathrm{d}}^{5\mathrm{p}}(k+1) - i_{\mathrm{d}}^{5}(k)}{T_{\mathrm{s}}}, \dfrac{di_{\mathrm{q}}^{5\mathrm{p}}}{dt} = \dfrac{i_{\mathrm{q}}^{5\mathrm{p}}(k+1) - i_{\mathrm{q}}^{5}(k)}{T_{\mathrm{s}}} \\ \dfrac{di_{\mathrm{d}}^{7\mathrm{p}}}{dt} = \dfrac{i_{\mathrm{d}}^{7\mathrm{p}}(k+1) - i_{\mathrm{d}}^{7}(k)}{T_{\mathrm{s}}}, \dfrac{di_{\mathrm{q}}^{7\mathrm{p}}}{dt} = \dfrac{i_{\mathrm{q}}^{7\mathrm{p}}(k+1) - i_{\mathrm{q}}^{7}(k)}{T_{\mathrm{s}}} \end{cases} \tag{15}$$

It should be noted that the above formula is not limited to the 5th ,7th harmonics and can be further expanded.

4.2.2 Traditional Prediction Model

In the block diagram, the conventional prediction model is incorporated to compare i_{d} , i_{q} , where harmonic extraction is performed, with $i_{\mathrm{d}}^{*}, i_{\mathrm{q}}^{*}$. The reason for the above consideration is that the given quantities have dynamic performance requirements, whereas if $i_{\mathrm{d}}^{'}$, $i_{\mathrm{q}}^{'}$ is used to compare with $i_{\mathrm{d}}^{*}, i_{\mathrm{q}}^{*}$, a further harmonic extraction of the given quantities of $i_{\mathrm{d}}^{*}, i_{\mathrm{q}}^{*}$ is required and the filtering present in this extraction not only elevates the computational latency even further, but also reduces the dynamic changes manifested as transient high order harmonics, thus reducing the dynamic performance.

The conventional prediction model is consistent with the equations described in Section 3 and is therefore not repeated here.

4.3 Synthetic Cost Function

The Synthetic Cost Function consists of the following three terms: the Base-wave Current Part, the Harmonic Current Part, and the Switching Frequency Limiting Part.The Base-wave Current Part and the Harmonic Current Part use traditional models and are therefore consistent with the description in Section 3, which will not be repeated in this section, but only illustrate the construction process of the Harmonic Current Part.The Harmonic Current Part value function is obtained by squaring and summing the predicted values of the harmonic currents obtained in section 4.2.1 and can be expressed as

$$\begin{aligned} g_{\mathrm{h}} = {} & \lambda_5\left(\left(i_{\mathrm{d}}^{5}(k+1)\right)^2 + \left(i_{\mathrm{d}}^{5}(k+1)\right)^2\right) \\ & + \lambda_7\left(\left(i_{\mathrm{d}}^{7}(k+1)\right)^2 + \left(i_{\mathrm{d}}^{7}(k+1)\right)^2\right) \end{aligned} \tag{16}$$

where λ_5 , λ_7 denotes the weighting coefficient of each harmonic term. It should be noted that according to the Fourier decomposition algorithm, the design of the weight coefficients should be $\frac{1}{n}$, where n represents the number of harmonics. In the actual simulation, due to the influence of perturbation and other variable characteristics, the above terms need to be adjusted according to the actual results. Through the above discussion, the overall formula of the integrated value function can be written as

$$\begin{cases} J = g_{\mathrm{b}} + g_{\mathrm{h}} + g_{\mathrm{s}} \\ g_{\mathrm{b}} = \left[i_{\mathrm{d}}^{*} - i_{\mathrm{d}}^{\mathrm{p}}(k+2)\right]^2 + \left[i_{\mathrm{q}}^{*} - i_{\mathrm{q}}^{\mathrm{p}}(k+2)\right]^2 \\ g_{\mathrm{h}} = \lambda_5\left(\left(i_{\mathrm{d}}^{5}(k+1)\right)^2 + \left(i_{\mathrm{d}}^{5}(k+1)\right)^2\right) \\ \qquad + \lambda_7\left(\left(i_{\mathrm{d}}^{7}(k+1)\right)^2 + \left(i_{\mathrm{d}}^{7}(k+1)\right)^2\right) \\ g_{\mathrm{s}} = \lambda_{\mathrm{f}} \sum_{i=a,b,c} \left|S_i(k) - S_i(k-1)\right| \end{cases} \tag{17}$$

 DOI:10.30420/566414044

When the Synthetic Cost Function is completed for all traversed vectors the voltage vector that minimizes the cost value *J* is obtained, i.e., the voltage vector issued at the moment *k+1*.

5 Simulation Verification Results

In order to validate the favorability of the proposed MPSHRC methodology, simulation experiments are carried out in Simulink for verification. The PMSM in the simulation is set to the real PMSM parameters and the parameter table is Table I.

TABLE I
Parameters of PMSM

Symbol	Value	Symbol	Value
U_{dc} (V)	310	P_N (kW)	1.25
R (Ω)	3.18	T_N (N-m)	5
L (mH)	8.5	n_N (r/min)	2000
ψ_f (Wb)	0.325	p	2

In all the experiments mentioned in this paper, the control frequency of the system is limited to 10 kHz. Thus it is possible to obtain that $T_s = 1\times10^{-4}$s .

TABLE II
Weighting Coefficients in Simulation

Motor Status	λ_f	λ_5	λ_7
2000rad/min,5N.m T-LSF-MPCC method	3	0	0
2000rad/min,5N.m MPSHRC method	4.5	0.5	0.14
500rad/min,5N.m T-LSF-MPCC method	2.6	0	0
500rad/min,5N.m MPSHRC method	3	0.25	0.14

In order to maintain the system in steady state operation at low switching frequencies, this paper agrees on the average switching frequency $\overline{f_L}$, which is specifically expressed as the average switching period per unit time of the six bridge arms of the power device. Since there is an unavoidable non-stationary characteristic of $\overline{f_L}$ under MPC control, a reference frequency datum $f_{sf} = 830\text{Hz}$ is delineated. The switching frequency weights λ_f are adjusted during the actual simulation to ensure that $\overline{f_L}$ is around f_{sf} . The final weighting factors used in the simulation are shown in TABLE II.

Experiments of the T-LSF-MPCC method with the proposed MPSHRC method at different rotational speeds were carried out under the above conditions and the results are shown in Fig.8 - Fig.11.

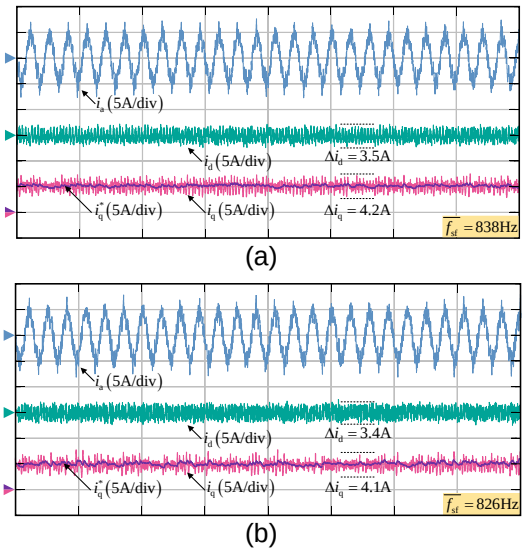

Fig. 8. Simulation results at rated torque (5N.m) and rated speed(2000rad/min), (a) T-LSF-MPCC method, (b) proposed MPSHRC method.

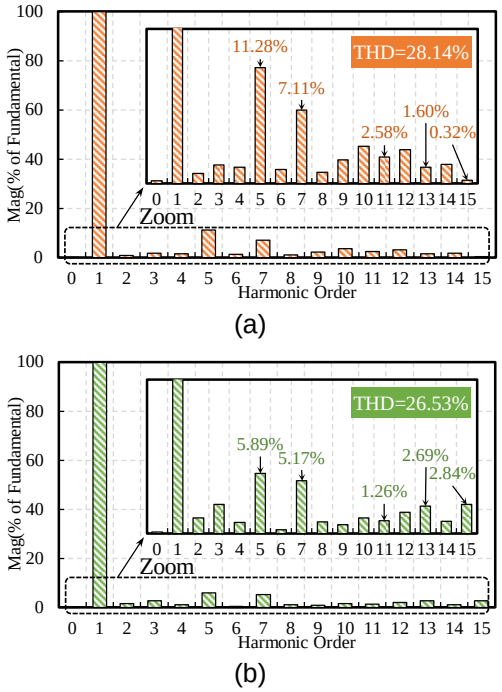

Fig. 9. FFT spectrum of phase current at rated torque (5N.m) and rated speed(2000rad/min), (a) T-LSF-MPCC method, (b) proposed MPSHRC method.

Fig.8 - Fig.9 show the experimental results of the motor at rated speed and rated load.

It can be seen that the current ripple of the T-LSF-MPCC method is more pronounced when the switching frequency is maintained near 830 Hz and also, its current Total Harmonic Distortion (THD) is 28.14%, which exhibits significant 5th as well as 7th harmonics in Harmonic order.

However, the proposed MPSHRC method has an unfavorable improvement on the above effect, and the current ripple realizes a slight reduction, and the THD is

reduced to 26.53%, and at the same time, the 5th, 7th, and 11th harmonics pointed out by the Harmonic order are reduced, in which the 5th harmonic reduction reaches 5.39%, the 7th harmonic reduction reaches 1.94%. Although the 11th harmonic is not suppressed, the reduction rate reaches 1.32%.The 13th and 15th high harmonics are increased respectively, which proves that the algorithm will promote a part of the stator current low harmonic content to the high harmonics when the motor is in rated condition.

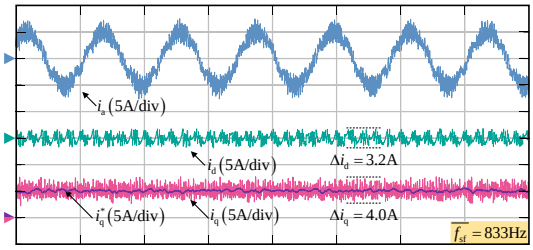

(a)

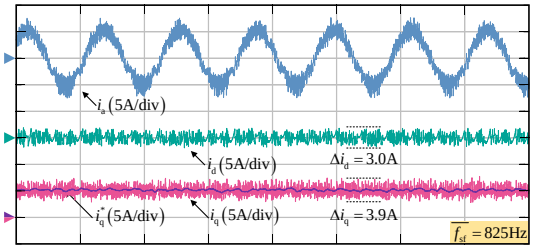

(b)

Fig. 10. Simulation results at rated torque (5N.m) and low speed(500rad/min), (a) T-LSF-MPCC method, (b) proposed MPSHRC method.

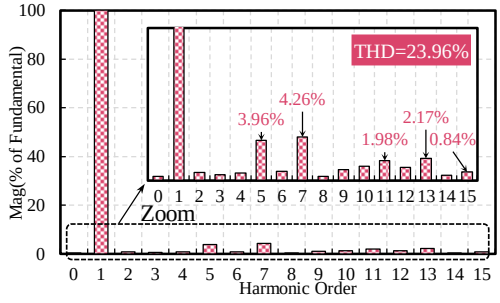

(a)

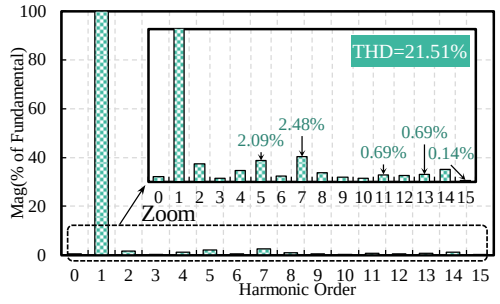

(b)

Fig. 11. FFT spectrum of phase current at rated torque(5N.m) and low speed(500rad/min), (a) T-LSF-MPCC method, (b) proposed MPSHRC method.

Fig.10 - Fig.11 shows the experimental results of the motor at rated torque and rated load. It can be seen that the proposed MPSHRC method maintains the superior results at low speed condition. both the Dq shaft currents are reduced with respect to the T-LSF-MPCC method.

The stator current THD is also reduced from 23.96% to 21.51% under the T-LSF-MPCC method, while the low harmonic content also has a significant improvement, with the 5th harmonic reduced by 1.87%, the 7th harmonic reduced by 1.78%, and the 11th harmonic reduced by 1.29%.

In conclusion, the feasibility of the proposed MPSHRC method in different states is verified by the load experiments of the motor in steady state.

6 Conclusion

Considering the impact of low harmonics on PMSMs operating at low switching frequencies, the text proposes a specific number of harmonics reduction method based on model predictive control.

The method extracts the corresponding harmonics using MSRFS and uses the next moment harmonic quantities predicted by a mathematical model of the PMSM considering the harmonics, and a synthetic cost function is designed to optimize the system in conjunction with a finite-set model predictive control.

Both demonstration and simulation validate the effectiveness of the proposed methodology and detailed data indications are given.

7 References

[1] X. Zhang, H. Bai and M. Cheng, "Model predictive control for PMSM drives with switching frequency optimization," 2021 IEEE 4th International Electrical and Energy Conference (CIEEC), Wuhan, China, 2021, pp. 1-6.

[2] X. Zhang, Y. Cao, C. Zhang and S. Niu, "Model Predictive Control for PMSM Based on the Elimination of Current Prediction Errors," in IEEE Journal of Emerging and Selected Topics in Power Electronics, vol. 12, no. 3, pp. 2651-2660, June 2024.

[3] Jinglin Liu, Chao Gong, Zexiu Han and Eryang Zhang, "An improved adaptive fuzzy PID controller for PMSM and a novel stability analysis method," 2017 IEEE 3rd International Future Energy Electronics Conference and ECCE Asia (IFEEC 2017 - ECCE Asia), Kaohsiung, 2017, pp. 2161-2164, doi: 10.1109/IFEEC.2017.7992386.

[4] C. He, H. Xiong and Z. Shen, "Current Loop Control Strategy of PMSM Based on Fractional Order PID Control Technology," 2021 6th Asia Conference on Power and Electrical Engineering (ACPEE), Chongqing, China, 2021, pp. 910-914.

[5] K. Ismail, T. D. Rachmildha, E. Rijanto, Y. Haroen and R. Ristiana, "Comparison of PID Controller Tuning Methods for Multi PMSM Angular Speed Synchronization," 2018 5th International Conference on Electric Vehicular Technology (ICEVT), Surakarta, Indonesia, 2018, pp. 95-99.

[6] X. Zhang and Z. Zhao, "Multi-Stage Series Model Predictive Control for PMSM Drives," in IEEE Transactions on Vehicular Technology, vol. 70, no. 7, pp. 6591-6600, July 2021.

[7] Y. Wang, Y. Zhu, X. Zhang, B. Tian, K. Wang and J. Liang, "Antidisturbance Sliding Mode-Based Deadbeat Direct Torque Control for PMSM Speed Regulation System," in IEEE Transactions on Transportation Electrification, vol. 7, no. 4, pp. 2705-2714, Dec. 2021.

[8] X. Zhang and C. Xu, "Second-Time Fault-Tolerant Topology and Control Strategy for the Open-Winding PMSM System Based on Shared Bridge Arm," in IEEE Transactions on Power Electronics, vol. 35, no. 11, pp. 12181-12193, Nov. 2020.

[9] Q. Wang, G. Wang, N. Zhao, G. Zhang, Q. Cui and D. Xu, "An Impedance Model-Based Multiparameter Identification Method of PMSM for Both Offline and Online Conditions," in IEEE Transactions on Power Electronics, vol. 36, no. 1, pp. 727-738, Jan. 2021, doi: 10.1109/TPEL.2020.3000896.

[10] X. Zhang and L. Xu, "A Simple Motor-Parameter-Free Model Predictive Voltage Control for PMSM Drives Based on Incremental Model," in IEEE Journal of Emerging and Selected Topics in Power Electronics, vol. 12, no. 3, pp. 2845-2854, June 2024, doi: 10.1109/JESTPE.2024.3387454.

[11] J. -D. Zhang, F. Peng, Y. -K. Huang, Y. Yao and Z. -C. Zhu, "A novel low control frequency control strategy of high switching frequency inverter for high speed PMSM current control," 2020 International Conference on Electrical Machines (ICEM), Gothenburg, Sweden, 2020, pp. 2358-2364.

[12] Q. Dong, B. Wang, Y. Yu, M. Tian, Z. Yun and D. Xu, "Hybrid PWM and Smooth Switching Technology for Traction PMSM Drives in Low Switching Frequency," 2020 IEEE 9th International Power Electronics and Motion Control Conference (IPEMC2020-ECCE Asia), Nanjing, China, 2020, pp. 2307-2312.

[13] Z. Chen, X. Huang, Y. Xu and J. Zhang, "Evaluation of the Harmonics in Permanent-Magnet Synchronous Traction Motor with Low Switching Frequency Power Supply," 2019 22nd International Conference on Electrical Machines and Systems (ICEMS), Harbin, China, 2019, pp. 1-4, doi: 10.1109/ICEMS.2019.8922206.

[14] S. Dai, J. Wang, Z. Sun and E. Chong, "Multiple Current Harmonics Suppression for Low-Inductance PMSM Drives With Deadbeat Predictive Current Control," in IEEE Transactions on Industrial Electronics, vol. 69, no. 10, pp. 9817-9826, Oct. 2022, doi: 10.1109/TIE.2022.3144577.

[15] B. Shao and Z. -Q. Zhu, "Optimal Selective Harmonic Elimination PWM for Dual Three-phase PMSM Under Low Switching Frequency," 2022 25th International Conference on Electrical Machines and Systems (ICEMS), Chiang Mai, Thailand, 2022, pp. 1-6, doi: 10.1109/ICEMS56177.2022.9983429.

[16] Y. -S. Jang and R. -Y. Kim, "Optimal Vector FCS-MPC in Multiple Paralleled Inverters System for PMSM," 2022 25th International Conference on Electrical Machines and Systems (ICEMS), Chiang Mai, Thailand, 2022, pp. 1-5.

[17] M. N. Uddin, M. M. Rashid, M. Rubaiyat, B. Hossain, S. M. Salam and N. A. Nithe, "Comparison of position sensorless control based back-EMF estimators in PMSM," 2015 18th International Conference on Computer and Information Technology (ICCIT), Dhaka, Bangladesh, 2015, pp. 5-10, doi: 10.1109/ICCITechn.2015.7488033.

[18] G. Liu, B. Chen, K. Wang and X. Song, "Selective Current Harmonic Suppression for High-Speed PMSM Based on High-Precision Harmonic Detection Method," in IEEE Transactions on Industrial Informatics, vol. 15, no. 6, pp. 3457-3468, June 2019, doi: 10.1109/TII.2018.2873652.